Biochar-induced Root Exudates Rewire the Rhizosphere Microbiome and Its Functionality

Hanyue Yang[1], Amina Furrkukh Mughal[2], Yaqi You[1,2,*]

[1]Department of Environmental Resources Engineering, SUNY College of Environmental Science and Forestry

[2]Graduate Program in Environmental Science, SUNY College of Environmental Science and Forestry

*Correspondence:

Yaqi You

402 Baker Lab, 1 Forestry Dr, Syracuse, NY 13210

E-mail: yyou@esf.edu

Phone: +1-315-470-6765

ABSTRACT

Biochar amendment has multifaceted benefits on the soil-plant system; yet the underlying mechanisms remain poorly understood. Integrating microfluidics and multi-omics and using wheat as a model plant, we demonstrate that biochar induces differential root exudation which rewires the rhizosphere microbiome and its functionality. Complex molecules in biochar-induced root exudates, particularly plant secondary metabolites and phytohormones, evoke a plant-beneficial rhizosphere microbiome centered by diverse plant growth promoting rhizobacteria (PGPR). Functionally, the restructured microbiome exhibits shifted nitrogen metabolism, characterized by enhanced nitrogen fixation and complete denitrification with reduced N_2O emission potential. Additionally, biochar suppresses methane production through orchestrated microbial community functional shifts, including stimulated methionine salvage that deprives the methanogenesis precursor methanethiol; suppressed biosynthesis of coenzyme M, a cofactor required for the methane-forming step; and an enrichment of methanotrophs and thus enhanced methane oxidation. The restructured microbiome also contributes to the transformation of phytohormones and biosynthesis of redox-active quinone compounds, having profound impact on the soil-plant system. Together, our work provides new insights into biochar's multifaceted roles in reprogramming the rhizosphere and highlights the promise of engineering the rhizosphere through reshaping root-microbe interactions using designed biochar or root exudate cocktails. Given the fact that fire-derived black carbon shares similar chemistry with biochar and that increased frequency of wildfire could cause more black carbon deposition, this research also spotlights the overlooked impact of fire-derived black carbon on belowground carbon and nitrogen dynamics through intricate rhizosphere interactions. New mechanisms unveiled in this research have implications for both sustainable agriculture and general soil biogeochemistry.

KEYWORDS: *biochar, multi-omics, root exudates, secondary metabolites, phytohormone, rhizosphere microbiome, plant growth promoting rhizobacteria, soil metabolome, nitrogen cycling, methane cycling*

INTRODUCTION

Sustainable soil management is vital for safeguarding food production, environmental health, and human well-being[1]. Biochar has been widely recognized as a multifunctional soil enhancer, capable of improving soil health, boosting crop productivity and stress resistance, reducing nutrient leaching, and mitigating greenhouse gas (GHG) emissions[2, 3]. These benefits are often attributed to biochar-induced changes in soil physicochemical properties, such as increased nutrient availability, enhanced water-holding capacity, reduced acidity or toxic substances[4, 5]. Emerging evidence, however, started to unveil more profound influence of biochar on the soil-plant system.

Soil is a dynamic living system, comprising diverse and complex microbial communities that drive numerous biogeochemical reactions[6]. Increasing evidence suggests that biochar amendment can alter microbial abundance, diversity, community structure, and functional compositions[5, 7]. However, few studies have investigated biochar's effects on the rhizosphere—a narrow, dynamic zone that serves as a critical interface between plant roots and soil microorganisms and a key component of the plant holobiont[2, 8, 9]. Our recent study found that biochar can modulate root endometabolites and rhizosphere microbiome[10]. But not all root endometabolites are secreted into the soil; root exudates that are actively secreted directly influence rhizosphere biogeochemistry and thus require further investigation.

Plants use root exudates to recruit plant-growth promoting rhizobacteria (PGPR) and thereby gain growth advantages such as enhanced resistance to diseases and stresses[11, 12]. Whether biochar induces root exudates favoring PGPR is still unknown. Further, nitrogen (N) is a key limiting nutrient for plant productivity in most terrestrial ecosystems, especially agroecosystems[13]. While biochar is reported to affect microbially mediated N cycling, including N fixation, nitrification, and denitrification, in bulk soil[14-16], its effect on rhizosphere N cycling is unclear. Specifically, biochar-induced root exudates may play an important yet understudied role therein[17, 18]. Unleashing biochar's potential in sustainable agriculture requires a mechanistic understanding of biochar's modulating effects on root exudation and the rhizosphere microbiome.

This study aimed to use wheat, a fertilizer-intensive cereal crop, as a model plant to elucidate biochar-induced chemical and biological shifts in the rhizosphere, with a focus on molecular mechanisms of biochar-induced rhizosphere reprogramming. Three specific objectives were: (1) identify biochar-induced root exudates, (2) characterize biochar-induced, root exudate-mediated rhizosphere microbiome restructuring, and (3) determine biochar's modulation on rhizosphere biogeochemistry, especially N and methane cycling. We conducted controlled experiments using laboratory-produced, well-characterized wheat biochar and a microfluidics device called EcoFAB (ecosystem fabrication), a modular growth system developed for studying the rhizosphere throughout plant development stages[19, 20]. We analyzed root exudates and the soil metabolome using untargeted metabolomics, the rhizosphere microbiome and its function using next-generation sequencing and real-time quantitative PCR (qPCR), and root exudate-microbe associations using a combination of network analysis and machine learning. Our work provides new mechanistic insights into biochar's multifaceted roles in reprogramming the rhizosphere and the potential of engineering the rhizosphere through reshaping root-microbe interactions.

MATERIALS AND METHODS

Biochar production and characterization

Biochar was produced by slow pyrolysis of wheat straw (350 °C for 30 min) with no oxygen in a laboratory reactor, the same as our prior work[10]. We chose low pyrolysis temperature due to the fact that biochar produced at lower pyrolysis temperatures tends to promote soil enzyme activity more than biochar produced at higher pyrolysis temperatures[2]. Biochar was characterized using scanning electron microscopy (SEM) for microscopic structure, energy-dispersive X-ray spectroscopy (EDS) for surface elemental composition, Fourier-transform infrared spectroscopy (FTIR) for molecular composition and functional groups, Boehm titration for three oxygen-containing functional groups (acidic carboxyl, lactone, and phenolic group) on the surface, and X-ray diffraction (XRD) for crystal structure, in addition to conventional analysis of pH, major and

98 trace elements, electrical conductivity, and cation exchange capacity (**Table S1**). Details are in
99 the Supporting Information (SI).
100
101 **EcoFAB fabrication**
102 We used EcoFAB devices, a fabricated ecosystem, for wheat plant cultivation, rhizosphere
103 observation, and sample collection[20]. This setting enables continuous investigation of the
104 rhizosphere under highly controlled conditions. We downloaded the original design files
105 (https://eco-fab.org/device-design/) and customized the design to accommodate wheat seedlings.
106 Acrylonitrile butadiene styrene (ABS) mold parts were fabricated using a MakerBot Replicator 2X
107 3D printer, acrylic mold parts were fabricated on a lathe machine, and the assembled mold was
108 used to cast polydimethylsiloxane (PDMS) layers (**Fig S1**)[21]. Our prototype EcoFAB device
109 consisted of a PDMS oval chamber (97.6 × 64 × 3.2 mm) adhering to a large rectangular coverslip
110 (102 × 76 × 1.2 mm) (Ted Pella) in an airtight way (**Fig S1**). Each device was enclosed in a
111 transparent cover box (**Fig 2A; Fig S1**) to maintain a sterile environment for plant experiment.
112 Before experiments, the EcoFAB chamber was rinsed with sterile Milli-Q water; the device surface
113 and the cover box were sterilized using 70% ethanol for 30 minutes and then 100% ethanol for 5
114 min. More details about EcoFAB fabrication and device assembly are in the SI.
115
116 **Plant experiment and sample collection**
117 In this study, we applied wheat biochar at a rate of 0.25% (w/w) based on cumulative
118 evidence that lower rates promote plant growth while higher rates inhibit growth and our prior
119 observations that wheat biochar at 0.25% rate yields unique rhizosphere alterations[10]. To prepare
120 soil slurries, 100 g of agricultural soil (**Table S1**) was added to 1 L sterile Milli-Q water, with or
121 without biochar. Soil slurries were shaken for 16 hours to reach thorough mixing, and slowly
122 injected into each EcoFAB chamber with a sterile syringe. Wheat (*Triticum aestivum* L.) seeds
123 were germinated and seedlings of similar sizes were transferred aseptically into sterilized EcoFAB
124 devices containing soil slurries with or without biochar (one plant per device; four biological

125 replicates for each treatment). Plants were cultivated under full spectrum LED light simulating
126 natural sunlight (12 hour light, 12 hour dark) and controlled humidity (80%) at 25 °C for 21 days,
127 and the development of root systems was monitored (**Fig S1**). Milli-Q water was added to EcoFAB
128 devices every three days to maintain humidity. To ensure reproducibility, the experiment was
129 conducted twice (8 EcoFAB devices in each independent round).

130 After 21 days, individual EcoFAB devices were dissembled, and remaining soil slurries
131 and plant seedlings were collected. Soil slurries were immediately stored at -80°C until metabolite
132 extraction, while seedlings were immediately processed to collect rhizosphere soils like in our
133 prior studies[10, 22]. After rhizosphere soil removal, individual plants with clean root surfaces were
134 transferred to sterile 15 mL centrifuge tubes containing 15 mL Milli-Q water to allow for exudation
135 for 24 hours like in our prior study[23]. An aliquot of the collected exudated solution (1.5 mL) was
136 transferred to a 2.0 mL sterile microcentrifuge tube, dried using a vacuum concentrator (Savant
137 SpeedVac SPD300DDA, Thermo Scientific), and 1.5 mL of methanol solution (80% v/v in Milli-Q
138 water) was added to the tube, followed by vortexing for 15 minutes and sonication bath for 5
139 minutes at room temperature. The resulting extract was filtered through a 0.22 μm PVDF filter
140 (Millipore) and stored at -80 °C until metabolomics analysis. Similar procedures were used to
141 extract soil exometabolites (detailed in the SI).

142

143 **Untargeted metabolomics**

144 Root exudates and soil slurries were analyzed using liquid chromatography-tandem mass
145 spectrometry (LC-MS/MS) performed on a Vanquish LC system in conjunction with a Q Exactive
146 HF Orbitrap LC-MS system[24] coupled with an electrospray ionization (ESI) source (Thermo
147 Fisher). The MS has a resolving power of up to 240,000 FWHM (Full Width at Half Maximum) at
148 500 m/z and a mass range of 20-1200 m/z. Extract aliquots of 10 μL were injected into a Hypersil
149 GOLD C18 column (1.9 μm, 2.1×150 mm) (Thermo Fisher) operated at 30 °C. LC mobile phases
150 consisted of solvent A (0.1% formic acid in Milli-Q water) and solvent B (0.1% formic acid in LC/MS
151 grade acetonitrile), and the flow rate was maintained at 300 μL/min. MS was operated in both

152 positive and negative ion mode (ESI+ and ESI-). More LC-MS details are in the SI.

153 Spectral data was processed as before[10]. Raw data was converted to the generic mzXML
154 format and processed using three platforms (MetaboAnalyst 6.0, XCMS, MZmine3)[25-27], and the
155 resulting feature tables were merged without redundancy and further processed in MetaboAnalyst
156 6.0 for functional analysis. Compounds were converted to the International Union of Pure and
157 Applied Chemistry (IUPAC) names and classified to the "Class" level of the purely structure-based
158 chemical taxonomy (ChemOnt) using ClassyFire[28]. Principal coordinates analysis (PCoA) was
159 performed based on Jaccard distance using the "vegan" package[29]. Significant fold change (FC)
160 was determined by the Mann-Whitney *U* test with Benjamini-Hochberg correction ($|\log_2 FC| > 1$
161 and $p < 0.05$). For network analysis, pairwise Pearson correlation with false discovery rate (FDR)
162 control was calculated using the "WGCNA" package[30]; only significant correlations ($r > 0.9$ and
163 adjusted $p < 0.01$) were retained. Network topology was assessed with the "igraph" package[31].
164 Node degree distributions were fitted to a power-law model, and nodes with degrees exceeding
165 the 95th percentile were identified as highly connected hub nodes[10].

166

167 **Next generation sequencing, qPCR, and biofilm assay**

168 Metagenomic DNA was extracted from rhizosphere soils using the ZymoBIOMICS
169 DNA/RNA Miniprep Kit following the manufacturer's protocol (Zymo Research). A PowerLyzer
170 Homogenizer was used to maximize extraction efficiency. The resulting DNA was assessed on a
171 Qubit 4 fluorometer with the 1× dsDNA High Sensitivity Assay Kit (Thermo Fisher) and by
172 electrophoresis. 16S rRNA gene sequencing and data processing were performed using QIIME2,
173 DADA2, and the "phyloseq" package as before[10, 22]. The "edgeR" (Empirical Analysis of Digital
174 Gene Expression in R) package was used to identify differential taxa between samples.
175 PICRUSt2 was used to infer metagenomic functional contents[32]; PICRUSt2 predictions were
176 subjected to differential abundance analysis using the R package "ggpicrust2"[33]. Microbial
177 community growth rate, i.e., median predicted minimum doubling time (mPMDT), was predicted
178 using the R package "gRodon"[34, 35]. Microbial network analysis was constructed using SparCC[36].

179 Community assembly mechanisms were assessed using the null model approach. We calculated
180 the β-nearest taxon index (βNTI) using the R package "iCAMP" to estimate the relative importance
181 of deterministic versus stochastic assembly processes[37], and calculated the Raup-Crick metric
182 using Bray-Curtis dissimilarities (RC_{BC}) to estimate the relative importance of selection, drift,
183 dispersal limitation, and homogenizing dispersion[38]. More details on sequencing and data
184 processing are in the SI.

185 While PICRUSt2 inference provides a more comprehensive snapshot of community
186 functions, inference accuracy varies. Therefore, we used qPCR to quantify the abundance of
187 eubacterial 16S rRNA gene (proxy of total bacteria) and key genes involved in nitrogen (*nifH*, *nxrA*,
188 *nirK*, *nirS*, *nosZ* Clade I) and methane (*mcrA*, *pmoA*) cycling using established primers (**Table**
189 **S2**). qPCR was performed on a CFX Duet Real-Time PCR System (BioRad) with SsoAdvanced
190 universal SYBR green supermix (Bio-Rad), 2 μL of DNA template (2-fold diluted to mitigate soil
191 matrix inhibition effect), and primers (0.48 μM each) in a 25 μL reaction volume. The thermal
192 program consisted of an initial denaturation at 95°C for 2 min, followed by 35 (16S, *mcrA*, *nxrA*)
193 or 40 (*nifH*, *nirK, nirS*, *nosZ*, *pmoA*) cycles of 10 sec at 95 °C, 20 sec at the annealing temperature
194 (**Table S2**), and 30 sec at 72 °C. A melting curve analysis was conducted after each run to verify
195 reaction specificity. Standard curves were generated using a cloned PCR product for 16S rRNA
196 gene and synthetic DNA (gBlocks, Integrated DNA Technologies) for other genes (**Fig S2**),
197 following the MIQE guidelines[39]. More details of qPCR and data processing are in the SI.

198 To test whether biochar-induced root exudates promote biofilm formation compared to root
199 exudates from control plants, we conducted a biofilm assay using a model soil bacterium
200 *Pseudomonas putida* KT2440[40]. The results were normalized against dissolved organic carbon
201 (DOC) content in root exudates to exclude the effect of varying C content (details in the SI).

202

203 **Multi-omics integration**

204 We used two approaches to identify associations between root exudates and rhizosphere
205 microbes: (1) OmicsNet 2.0 which utilizes multiple databases to create multi-omics networks, and

206 (2) mmvec (microbe-metabolite vectors), a neural network approach that predicts an entire
207 metabolite profile from a single microbe sequence[41, 42]. OmicsNet 2.0 calculates metabolite-
208 microbe correlations based on microbial metabolic capacity and pertinent proteins that are
209 predicted using high-quality genome-scale metabolic models. The mmvec approach estimates
210 the conditional probability of observing a metabolite given that a microbe is present to identify the
211 most likely metabolite-microbe interactions. Compared to approaches based on correlation (e.g.,
212 Spearman's) or network (e.g., SparCC), mmvec can identify previously undiscovered patterns
213 and is less prone to false discovery (positive or negative) as it provides consistency between
214 absolute and relative abundances of compositional data. However, mmvec does not calculate the
215 statistical significance or confidence interval of each metabolite-microbe pair. Here we combined
216 the two approaches to maximize the discovery of true metabolite-microbe interactions. The highly
217 co-occurring 10 root exudates and 12 microbial genera, identified by both approaches, were
218 visualized using a heatmap. Similar approaches were used to identify and visualize associations
219 between rhizosphere microbes and soil exometabolites. More details are in the SI.
220

221 **General statistics and data visualization**

222 Bioinformatics, statistics, and data visualization were performed in R (4.2.1) and Python
223 (3.7) with various R packages and Python modules. Significant differences were determined using
224 one-way analysis of variance (ANOVA) or Welch's *t* test, nonparametric statistics (Wilcoxon or
225 Kruskal-Wallis), and permutational multivariate analysis of variance (PERMANOVA), depending
226 on the variable. Network visualization used Gephi (0.10.1) and Cytoscape (3.9.1). More details
227 are in the SI.
228

229 **RESULTS AND DISCUSSION**

230 **1. Biochar significantly promotes wheat plant growth**

231 SEM indicated the wheat biochar used here had a porous morphology (**Fig 1A**). FTIR
232 spectra showed the biochar contained aromatic compounds (particularly those with benzene rings

233 and quinone groups), C–O bonds from esters or ethers, nitriles, silicates and/or carbonates, and
234 possibly C–N or P–O (**Fig 1B; Fig S3**) (more details in the SI)[43-45]. EDS analysis revealed the
235 surface of the biochar predominantly contained C (62.36%), O (24.52%), Si (6.13%), K (3.06%),
236 and Ca (1.04%) (averaged atomic%, n = 29) (**Fig 1C**). Consistent with the EDS results, XRD
237 spectrum indicated the presence of amorphous C, graphite, and various mineral crystals
238 containing Si, K, and Ca (**Fig 1D**) (more details in the SI)[44, 46]. These results reflected the biochar's
239 feedstock (wheat straw) and the production condition (slow pyrolysis at 350 °C).

240 In the 21-day EcoFAB experiment (**Fig 2A**), application of 0.25% (w/w) wheat biochar
241 yielded 1.59 times more fresh weight of shoots (Welch *t* test: $p < 0.001$) (**Fig S4**). Fresh weight of
242 roots had no significant difference (Welch *t* test: $p = 0.413$), but biochar-treated plants had more
243 lateral roots (**Fig S4**). These results are consistent with our prior 15-day pot study[10] and suggest
244 biochar may promote wheat growth more significantly in larger systems.

245

246 **2. Biochar induces differential root exudation**

247 Biochar induced differential root exudation (**Table S3**), as shown by PCoA of Jaccard
248 distance of 312 exudate compounds detected across samples from two independent rounds of
249 EcoFAB experiments (PERMANOVA: $p = 0.145$ for round x treatment) (**Fig S5**). This is due to
250 systematic regulation of root metabolism by biochar, as evidenced by increased average degree
251 and centrality of root exudate co-occurrence network (**Fig S6**). Specifically, biochar significantly
252 regulates carbohydrate metabolism, glycan biosynthesis, the metabolism of terpenoids and
253 polyketides, and nucleotide metabolism, all of which are highly involved in plant growth and
254 development, signaling, and stress defense[47-49].

255 Among the 312 exudate compounds, six compounds were only identified in biochar-
256 induced root exudates, including two flavanonols, one flavanone and its direct precursor, a
257 phenolic ester, and dUMP (**Table S3**). Further, biochar significantly affected 39 compounds
258 ($|Log_2FC| > 1$, *p-adjusted* < 0.05) from 14 ChemOnt classes: 10 organooxygen compounds, 6
259 flavonoids, 3 prenol lipids, 3 fatty acyls, 2 from each of four classes (organonitrogen compounds,

260 steroids and steroid derivatives, imidazopyrimidines, carboxylic acids and derivatives), 1 from
261 each of five classes (5'-deoxyribonucleosides, pyrimidine nucleotides, furanoid lignans, linear 1,3-
262 diarylpropanoids, organic phosphoric acids and derivatives), and 4 unclassed chemicals (**Fig 2B**).
263 Three compounds having regulatory roles in plant defense were upregulated, namely beta-1,4-
264 poly-N-acetyl-D-glucosamine (chitin) (2.2 fold), (22S)-22-hydroxycampest-4-en-3-one (a direct
265 precursor of brassinosteroids (BRs)) (2.6 fold), and 2,4-dihydroxy-1,4-benzoxazin-3-one-
266 glucoside (DIBOA-Glc, a benzoxazinoid (BX) compound) (5.2 fold). Chitin enhances plant
267 immune responses by activating defense-related genes as an elicitor while chitin decomposition
268 by-products also inhibit pathogen[50]. BRs are phytohormones indispensable for root growth and
269 BR biosynthesis is largely restricted to the root elongation zone[51]. DIBOA-Glc is the glycosylation
270 product of DIBOA, the most abundant BX in cereal crops, and the precursor of defense-active
271 compound DIMBOA-Glc. BX glucosides are stored in vacuoles and released over time to the
272 rhizosphere where their derivatives can suppress weeds and hostile microbes while enriching
273 beneficial microbes[52-54]. Our results indicate that biochar promotes plant growth by upregulating
274 root exudates that have antimicrobial and antioxidant activities. Further, BRs and BXs are
275 secondary metabolites known for their signaling functions, and increasing evidence reveals they
276 also mediate plant-microbe interactions such that shifts in their biosynthesis can reshape the
277 rhizosphere microbiome [52, 54, 55]. Here, by upregulating biosynthesis of plant signaling metabolites,
278 biochar may modulate the rhizosphere microbiome, which indeed occurred as discussed later.
279 Thirty-six root exudates were downregulated, including six flavonoids. Flavonoids are essential in
280 plant fitness and rhizosphere microbiome assembly[56]. Downregulation of flavonoid biosynthesis
281 could reflect either reduced stress due to scavenging of reactive oxygen species (ROS) or BR-
282 induced inhibition of flavonoid biosynthesis[57]. It may also reflect shifted flavonoid biosynthesis as
283 several flavonoids, including 2 flavanonols (dihydrokaempferol, (+)-2,3-dihydrofisetin), one
284 flavanone and its direct precursor (eriodictyol and eriodictyol chalcone), and a phenolic ester (4-
285 coumaroylshikimate) were only detected in biochar-treated root exudates. Overall, our results
286 provide chemical insights into widely observed biochar benefits on plant productivity[58].

287 A majority (81.4%) of the 312 exudate compounds were previously detected inside of root
288 tissues (**Fig S7**; also see the SI text)[10]. But we also identified 58 exudate compounds that were
289 not detected within root tissues, including 8 fatty acyls, 6 organooxygen compounds, 5 pyrimidine
290 nucleotides, 5 purine nucleotides, 4 carboxylic acids and derivatives, 3 flavonoids, 1 isoflavonoid,
291 3 prenol lipids, among others, such as DIBOA-Glc and gibberellin A29-catabolite (GA29-catabolite,
292 a deactivated catabolite from GA20) (**Fig S7; Table S4**). These 58 actively exudated compounds
293 likely have critical roles in the rhizosphere: Fatty acyls and prenol lipids, organooxygen
294 compounds, carboxylic acids and derivatives, and flavonoids and isoflavonoids are involved in
295 rhizosphere signaling and able to mediate plant root-microbe interactions[56, 59, 60]. Among the
296 detected fatty acyls, linolenic acids are plant defense signaling molecules[61]; 2'-deoxymugineic
297 acid is an iron (III) phytosiderophore, influencing rhizosphere microbiome composition through
298 iron competition[9, 62]. Five of the six detected organooxygen compounds were inositol phosphates,
299 a major pool of organic phosphorus in soil and signaling molecules mediating microbial root
300 colonization[63]. These results, along with our prior pot study[10], unveil biochar-induced metabolic
301 alterations in roots and subsequent exudation of molecules with profound modulating effects on
302 plant root-microbe interactions.
303
304 **3. Biochar-induced root exudates drive the rhizosphere microbiome restructuring**
305 ***3.1. Biochar rewires the rhizosphere microbiome and microbial interactions***
306 In the native wheat rhizosphere, the top 10 phyla and top 40 genera comprised 60% and
307 35% of all prokaryotes, respectively, reflecting the core rhizosphere microbiome of plant,
308 especially cereals[9]. Biochar had limited influence on rhizosphere microbial alpha diversity but
309 considerably altered microbiome composition (PERMANOVA test: $p = 0.001$ for round $\times$ treatment)
310 (**Fig 3A**), promoting 12 genera while suppressing 9 genera (**Fig S8-S9; Table S5**) (more details
311 in the SI).
312 Remarkably, biochar enhanced microbial interactions, evidenced by greater microbial
313 network modularity and centrality, and a large number of new keystone genera emerged (60 vs.

314 53 in the treated vs. native rhizosphere) (**Fig 3C; Fig S10; Table S6-S8**). Twelve common
315 keystone bacterial genera were observed in the native and treated rhizosphere (detailed in the
316 SI), including nine PGPR from Actinobacteria, Alphaproteobacteria and Gammaproteobacteria:
317 *Bradyrhizobium* and *Microvirga* are N-fixing bacteria[64]; *Paracoccus* is capable of metabolizing
318 nitrogen, nitrate, and ammonia[65]; *Lysobacter* and *Stenotrophomonas* can suppress soil-borne
319 pathogens by producing lytic or antimicrobial substances[66, 67]; *Shinella* can degrade polycyclic
320 aromatic hydrocarbons[68]; *Cellvibrio* has an extensive repertoire of carbohydrate-active enzymes
321 for degrading polysaccharides (cellulose, dextran, xylan, chitin, and starch), thus enhancing
322 organic matter turnover[69, 70]; *Rhodococcus* contributes to nutrient cycling[71] and influences plant
323 stress response by metabolizing the phytohormone abscisic acid (ABA)[72]; *Solirubrobacter* can
324 produce the phytohormone indole-3-acetic acid (IAA) and improve nutrient bioavailability through
325 assimilatory reduction of sulphate and utilizing a wide range of carbohydrates[73] (more in the SI).
326 Besides these common keystone genera, the native rhizosphere microbiome had classic
327 rhizosphere keystone genera, such as those able to degrade plant cell wall polysaccharides
328 (details in the SI), whereas the biochar-treated rhizosphere had additional diverse PGPR as
329 keystone genera (**Fig 3C**). One example was *Chryseobacterium* (with greatest betweenness and
330 closeness centrality) that can enhance plant nutrient acquisition, degrade aromatic compounds,
331 produce antioxidant enzymes, synthesize IAA, and lower plant stress levels by reducing the
332 immediate precursor of the stress phytohormone ethylene using 1-aminocyclopropane-1-
333 carboxylate (ACC) deaminase[74]. Another example was methylotrophic
334 *Methylobacterium*/*Methylorubrum* (connector hub) that can synthesize developmental
335 phytohormones (auxins, gibberellins, cytokinins) and ACC deaminase and fix nitrogen[75]. Other
336 keystone PGPR genera in the biochar-treated rhizosphere included N-fixers *Allorhizobium-*
337 *Neorhizobium-Pararhizobium-Rhizobium* and *Azospirillaceae*, denitrifiers *Magnetospirillum*[76, 77],
338 *Nocardia* able to produce IAA[78, 79], Planctomycetes *OM190* (module hub) able to produce diverse
339 secondary metabolites including antimicrobial compounds[80], and *Solibacillus* that can produce
340 IAA and plant singling molecule hydrogen cyanide and secrete siderophores to solubilize or

341 chelate minerals[81, 82].

342 These results reveal a new microbial mechanism for the widely-reported but poorly-
343 understood plant-promoting effect of biochar: Biochar elicits diverse PGPR, including nitrogen
344 fixers, denitrifiers, and phytohormone producers, to emerge as microbiome keystone taxa.
345 Phytohormones like auxins, gibberellins, and cytokinins regulate plant growth and development
346 (e.g., cell division and differentiation, root branching), immunity, and abiotic/biotic stress
347 responses[83, 84]; therefore, the biochar-treated rhizosphere microbiome may grant the plant with
348 multiple benefits. Indeed, while we did not track phytohormone dynamics, we observed higher
349 shoot mass and more lateral roots of biochar-treated plants (**Fig S4**), a phenomenon likely
350 attributed to the enrichment of phytohormone-producing PGPR and the aforementioned
351 upregulation of plant BRs biosynthesis. Given the significance of keystone taxa in overall
352 microbiome structure and functioning[85], future research should directly measure microbial
353 processing of phytohormones in the biochar-treated rhizosphere.

354

355 ***3.2. Rhizosphere microbiome rewiring is linked to biochar-induced root exudates***

356 Plants use root exudates to recruit and tune the rhizosphere microbiome[9]. Since biochar
357 induced differential exudation, particularly polyphenols and lipids, we hypothesized that shifts in
358 root exudate chemistry restructured the rhizosphere microbiome, selectively enriching or
359 suppressing specific bacterial taxa, through metabolic coupling of biochar-induced root exudates
360 with microbial substrate-use preferences as suggested by recent evidence from laboratory
361 experiments and genome-informed trait-based modeling[86-88]. In line with this hypothesis, the
362 biochar-rewired rhizosphere microbial community had a slower growth rate than the native
363 microbiome (**Fig 3D**), suggesting a switch from higher growth and lower substrate utilization
364 efficiency to lower growth and higher substrate utilization efficiency[86, 87]. To validate this genome-
365 informed, community-level prediction, we tested biofilm formation of a model soil bacterium *P.*
366 *putida* KT2440 under exposure to normal or biochar-induced root exudates (**Fig S11A**). While
367 root exudates from control and biochar-treated plants had similar levels of DOC (**Fig S11C**) (p =

368 0.607), biochar-induced root exudates resulted in less *P. putida* biofilm within 48 hours (**Fig S11B**)
369 (p = 0.004), consistent with our hypothesis that biochar-induced root exudates favor slow-growing
370 microbes capable of utilizing complex molecules. It should be noted that this shift did not
371 significantly change the total bacteria number. Instead, biochar insignificantly increased the
372 number of rhizosphere bacteria as shown by qPCR results (**Fig S12**). Analysis of community
373 assembly mechanisms found that dispersal limitation dominated rhizosphere community turnover
374 (63.11% of all assembly mechanisms) (**Fig S13A-B**), suggesting low dispersal rates in the
375 rhizosphere niche where weak or unstructured selective pressures from substrate utilization
376 enable high compositional turnover[89]. Together, computational prediction, biofilm assay, and
377 community assembly analysis support our hypothesis that biochar rewired the rhizosphere
378 microbiome through metabolic coupling of biochar-induced root exudates with microbial
379 substrate-use preferences.

380 Our hypothesis is further supported by the coincidence of biochar-enriched root exudate
381 composition, including chitin and DIBOA-Glc, and the enrichment of bacteria having chitinolytic
382 activity and BXs-enhanced growth (detailed in the SI). This motivated us to explore specific
383 microbe-exudate compound associations. Combining the co-occurrence network (OmicsNet 2.0)
384 and neural network (mmvec) approaches, we identified 12 bacterial genera, including 11 PGPR
385 (*Bacillus*, *Blastococcus*, *Bradyrhizobium*, *Brevundimonas*, *Mesorhizobium*, *Nevskia*,
386 *Paenibacillus*, *Pantoea*, *Pseudomonas*, *Rhodococcus*, *Roseomonas*)[90, 91], with highest
387 associations with biochar-induced root exudates (mainly plant secondary metabolites) (**Fig 4; Fig**
388 **S13C**). Extremely high co-occurrence probability may manifest when a compound is a preferred
389 substrate to certain bacteria and multiple lines of evidence support the metabolic coupling nature
390 of the observed microbe-exudate compound associations[54, 86-88].

391 Four flavonols, including three quercetin derivatives and one kaempferol derivative, had
392 varying co-occurrence with the 12 bacterial genera: Isoquercitrin (quercetin 3-O-glucoside) had
393 very high co-occurrence with all the 12 genera, particularly *Pantoea*; quercetin 3-O-rhamnoside-
394 7-O-glucoside and kaempferol-3-O-rhamnoside had similar co-occurrence patterns with several

395 microbes, opposite to quercitrin (quercetin 3-O-rhamnoside). Quercetin and its derivatives can
396 stimulate PGPR and bacteria like *Pantoea* harbor quercetin dioxygenases for degrading
397 flavonols[56, 92]. This aligns with our observation of very high co-occurrence probabilities between
398 *Pantoea* and two quercetin derivatives (quercitrin > isoquercitrin). Three gibberellins (GAs),
399 GA12-aldehyde (early precursor of bioactive GAs), GA44 open lactone (key intermediate in
400 bioactive GA1 synthesis), and GA34-catabolite (deactivated catabolite from bioactive GA4), had
401 varying co-occurrence with the 12 bacterial genera, with GA44 open lactone and GA34-catabolite
402 showing opposite patterns. GA phytohormones are crucial for many aspects of plant growth and
403 development. Appropriate levels of bioactive GA are tightly regulated in plants and also modulated
404 by PGPR such as *Bacillus*, *Bradyrhizobium*, and *Mesorhizobium* that possess GA metabolic
405 pathways[93-95]. Here *Bacillus* co-occurred with GA34-catabolite, while *Bradyrhizobium* and
406 *Mesorhizobium* had very high co-occurrence probability with GA44 open lactone and GA34-
407 catabolite, respectively, suggesting their involvement in GA metabolism. (S)-Abscisic acid, the
408 naturally occurring and bioactive form of phytohormone ABA, and its direct catabolite 8'-
409 hydroxyabscisic acid had high co-occurrence with *Blastococcus*, *Bradyrhizobium*, and
410 *Roseomonas*, suggesting ABA metabolism by these bacteria. Indeed, PGPR like *Bradyrhizobium*
411 can regulate ABA levels in the rhizosphere through biosynthesis and catabolism of ABA [52, 94, 96, 97].
412 Two glycosides of phytohormone cytokinins, cis-zeatin-O-glucoside and dihydrozeatin-O-
413 glucoside, had opposite patterns, with cis-zeatin-O-glucoside showing very high co-occurrence
414 with several PGPR (*Mesorhizobium* > *Rhodococcus* > *Pseudomonas* > *Bacillus*). It is known that
415 *Rhodococcus* and *Pseudomonas* can produce cytokinins[94, 98, 99].
416 Taken together, our results reveal biochar-induced root exudates as a key driver reshaping
417 the rhizosphere microbiome, likely through metabolic coupling of root exudates with microbial
418 substrate-use preferences. In particular, secondary metabolites such as flavonoids (flavonols)
419 and developmental phytohormones (GAs, ABA, cytokinins) evoke diverse PGPR capable of
420 utilizing these secondary metabolites. Our study thus provides a new chemical mechanism for
421 the widely-reported but poorly-understood plant-promoting effect of biochar. Further research

422 employing metagenomics and metatranscriptomics is required to ascertain our observations and
423 elaborate underlying metabolic mechanisms.
424
425 **4. Biochar-treated rhizosphere microbiome has shifted functions**
426 ***4.1. Shifted N and methane cycling***
427 Many studies have reported biochar's impact on bulk soil N and methane cycling[2, 3]. We
428 speculate such effects, likely due to changes in microbial functional composition and metabolic
429 pathway, can also occur in the rhizosphere. qPCR measurements found increased abundance of
430 *nifH* (N fixation), *nxrA* (nitrification, NO_2^- to NO_3^-), *nirS* (denitrification, NO_2^- to NO) and *nosZ*
431 (denitrification, N_2O to N_2), and reduced abundance of *nirK* (denitrification, NO_2^- to NO) in biochar-
432 treated rhizosphere (*p*-adjusted > 0.05) (**Fig 5B**). Increases in N fixation and nitrification genes
433 due to biochar treatment were also detected by community-level function prediction using
434 PICRUSt2 (**Fig S14**) (detailed in the SI). These trends are consistent with the emergence of N-
435 fixing bacteria (e.g., *Allorhizobium-Neorhizobium-Pararhizobium-Rhizobium*, *Azospirillaceae*) as
436 keystone taxa and the enrichment of ammonia-oxidizing bacteria (e.g., *Nitrosomonas*) in the
437 biochar-treated rhizosphere (**Fig 3C**; **Table S5**). Interestingly, biochar-induced increase in *nxrA*
438 gene coincided with a drastic enrichment of *Roseomonas*, a genus known to harbor *nxrA*[100] and
439 showing high co-occurrence with biochar-induced-phytohormone ABA (a terpenoid) and its direct
440 catabolite 8'-hydroxyabscisic acid (**Fig 4**). In complete denitrification, NO_2^- is transformed to NO
441 by nitrite reductases (*nirK* and *nirS*), while NO is further reduced to N_2O by nitric oxide reductases
442 (*nor*) and N_2O reduced to N_2 by nitrous oxide reductase (*nosZ*)[101]. Changes in the relative
443 abundance of these genes are associated with the production and consumption of N_2O and thus
444 the emission of this strong GHG. Specifically, the (*nirK*+*nirS*)/*nosZ* gene ratio has been used to
445 estimate N_2O emission potential[102]. Our qPCR results indicate a reduced (*nirK*+*nirS*)/*nosZ* ratio
446 in biochar-treated rhizosphere, indicating a promotion of complete denitrification and a reduction
447 of net N_2O emissions, likely due to biochar's role in facilitating electron transfer to denitrifying
448 microbes[103]. qPCR results also showed a reduction in the (*nirK*/*nirS*) ratio, suggesting a shift from

449 *nirK*-type nitrifiers, which often lack the *nosZ* gene, to *nirS*-type nitrifiers[104]. This observation is
450 consistent with the emergence of *Magnetospirillum* as keystone taxa and the enrichment of
451 *Sporomusa* in the biochar-treated rhizosphere (**Fig 3C**; **Table S5**). *Magnetospirillum* harbors a
452 complete denitrification pathway, able to reduce NO_3^- to N_2[105]. It should be noted that *Sporomusa*
453 species contain a recently-characterized novel lactonase-type N_2O reductase that cannot be
454 captured by existing primers[106]. Overall, these qPCR results align with prior observations from the
455 bulk soil that biochar promotes nitrogen fixation and nitrification while mitigating N_2O emissions[2],
456 and unveil microbiome restructuring as the underlying mechanism.

457 Neither qPCR or PICRUSt2 detected *mcrA* encoding the methyl-coenzyme M reductase
458 complex in any sample, reflecting the low representation of methanogens in the ectorhizosphere;
459 meanwhile, function prediction suggested that biochar suppressed coenzyme M biosynthesis I
460 required for methanogenesis (**Fig 5A**)[107]. Both qPCR and PICRUSt2 found increasing *pmoA*
461 (encoding membrane-bound particulate methane monooxygenase) in the biochar-treated
462 rhizosphere, indicating stimulated methane oxidation (**Fig 5B; Fig S15**)[108]. Consistently, two
463 exometabolites, isopentenyl pyrophosphate and dimethylallylpyrophosphate, were only present
464 in the biochar-treated rhizosphere (**Fig 5C; Table S12**). These two prenol lipids are five-carbon
465 building blocks for all isoprenoids, including bacteriohopanepolyols that are crucial structural
466 components of methanotroph membranes. Further, PICRUSt2 results showed biochar enriched
467 the methionine salvage pathway by >1000 fold (**Fig 5A**). In a sulfur-adequate environment like
468 here (**Table S1**), stimulated methionine salvage pulls 5-methylthioribulose-1-phosphate (MTRu-
469 1-P) towards L-methionine biosynthesis, limiting bioavailable methanethiol for archaeal
470 methanogenesis. Indeed, MTRu-1-P and its upstream precursor S-adenosylmethioninamine were
471 detected in root exudates, while MTRu-1-P downstream product 3-methylthiopropionic acid and
472 S-adenosylmethioninamine were detected in the soil metabolome (**Table S3; Table S12**). In
473 biochar-treated rhizosphere, microbial cysteine and methionine metabolism was significantly
474 associated with these root exudates and soil exometabolites (*p-adjusted* < 0.05) (**Table S9; Table**
475 **S13**), and four PGPR (*Roseomonas* > *Nevskia* > *Blastococcus* > *Bacillus*) had high co-occurrence

476 with 3-methylthiopropionic acid (**Fig S18**). Collectively, our results from qPCR, function prediction,
477 and untargeted metabolomics suggest that in the rhizosphere, biochar inhibits methane emission
478 through orchestrated microbiome functional shifts that are more complicated than previously
479 understood: stimulated methionine salvage that deprives the methanogenesis precursor
480 methanethiol; suppressed biosynthesis of coenzyme M, a cofactor required for the methane-
481 forming step; and enhanced methane oxidation.

482 Collectively, our results reveal new mechanisms of biochar's inhibition of two strong GHGs
483 in the rhizosphere, indicate the pivotal role of biochar-induced changes in root exudate chemistry
484 in restructuring the rhizosphere microbiome and its functionality, and identify PGPR genera whose
485 response to biochar-induced root exudates likely contributes to the observed shifts in N and
486 methane cycling.

487

488 ***4.2. Broader changes in rhizosphere microbiome functions***

489 A total of 506 exometabolites were detected in rhizosphere soils, including 180
490 compounds detected in root exudates collected by hydroponic secretion and 326 compounds only
491 found in the soil metabolome (**Fig S16; Table S12**). The 326 exometabolites consisted of
492 compounds secreted by roots in contact with rhizosphere microbes and microbial metabolites.
493 For example, DIBOA-Glc was only present in hydroponic secretion (**Fig 2B**), while its active form
494 DIBOA was only present in soil exometabolites and had high co-occurrence probability with 7
495 PGPR (**Fig S18**), likely reflecting BXs being used as recruitment signals for specific beneficial
496 microbes[52-54]. Various GAs were present in both root exudates and soil metabolites, but an early
497 precursor of bioactive GAs (GA12-aldehyde) was only present in root exudates, whereas two GA
498 catabolites (GA8, GA8-catabolite) and one intermediate (GA24) were only present in the soil
499 metabolome (**Table S12**), with GA24 showing high co-occurrence probability with numerous
500 PGPR, especially *Bradyrhizobium* known to possess GA metabolic pathways (**Fig S18**)[93-95].

501 Biochar significantly affected the soil metabolome chemistry (PERMANOVA: $p < 0.05$ for
502 treatment) (**Fig S17**), reflected in 64 most discriminative compounds ($|Log_2FC| > 1$, *p-adjusted* <

503 0.05) from 14 ChemOnt classes (**Fig 5C**) (detailed in the SI). Remarkably, several plant defense
504 compounds, including lotaustralin and methylthioalkylmalates (derived from methionine and
505 important precursors of sulfur-containing glucosinolates), were only present in biochar-treated
506 rhizosphere (**Fig 5C; Table S12**). Further, IAA and an indole derivative (5-
507 hydroxyindoleacetaldehyde) were present in the control rhizosphere but absent in biochar-treated
508 rhizosphere where 5-hydroxyindoleacetic acid, a direct oxidation product of 5-
509 hydroxyindoleacetaldehyde was detected, suggesting microbial metabolism of IAA and consistent
510 with aforementioned enrichment of IAA-producing PGPR (**Fig 5C; Table S3; Table S12**).

511 After mapping soil exometabolites to predicted microbial pathways (**Table S13**) and
512 comparing root exudate-microbe co-occurrence with microbe-exometabolite co-occurrence
513 (**Table S9**), we found biochar likely promoted microbial synthesis of phylloquinone and
514 menaquinol (more in the SI). Specifically, the menaquinol percussor 2-succinyl-5-enolpyruvyl-6-
515 hydroxy-3-cyclohexene-1-carboxylic acid was only present in root exudates, and its immediate
516 metabolites (1R,6R)-6-hydroxy-2-succinylcyclohexa-2,4-diene-1-carboxylate and 2-
517 succinylbenzoate were only present in the soil metabolome (**Table S3; Table S12**). Biochar
518 significantly reduced these two intermediates of menaquinone biosynthesis (**Fig 5C**).
519 Coincidentally, according to function prediction, biochar increased all but one menaquinone
520 biosynthesis gene (**Fig S19**). Menaquinol, the bioactive reduced form of menaquinone, was
521 detected in the soil metabolome, which can serve as an extracellular electron donor in the
522 rhizosphere environment. This may explain biochar-promoted complete denitrification observed
523 in this study and biochar-facilitated electron transfer as proposed by others[103].

524 Overall, these results from integrating multi-omics data indicate biochar's profound
525 modulating effects on the rhizosphere microbiome functionality, ranging from phytohormone
526 transformation attributed to biochar-enriched PGPR to biosynthesis of redox-active quinone
527 compounds. These changes have significant implications for plant development and soil
528 biogeochemistry. Future research should employ metagenomics and metatranscriptomics to
529 validate our observations and elaborate underlying microbiology mechanisms.

5. Environmental Implications and Significance

The research community is striving to develop sustainable technologies to support crop production while reducing GHG emissions and reliance on agrochemicals. The rhizosphere microbiome plays an essential role in plant growth and general soil biogeochemistry, and rhizosphere engineering has attracted increasing interest as a promising approach for sustainable agriculture. While biochar is a promising multifunctional soil conditioner, its effect on the rhizosphere is unknown. This study is among the first that elaborates biochar-induced root exudates as a key driver that rewires the rhizosphere microbiome and its functionality. By integrating multi-omics, we reveal new microbial and chemical mechanisms behind the widely reported but poorly understood biochar effects on the soil-plant system. Complex molecules in biochar-induced root exudates, including a wide range of plant secondary metabolites and phytohormones, evoke a plant-beneficial rhizosphere microbiome centered by diverse PGPR. The restructured microbiome is enhanced in N fixation, complete denitrification, methionine salvage, and methane oxidation, thus suppressing N_2O and CH_4 emissions. The restructured microbiome also contributes to the transformation of phytohormones and biosynthesis of redox-active quinone compounds, with critical implications for the soil-plant system. Future research should apply integrated metagenomics/metatranscriptomics, leverage larger-scale and field experiments, and investigate other plant models to validate and extend our findings. Future research should also directly demonstrate biochemical connections between the root exudate compounds and PGPR identified in this study. Nevertheless, this research provides new insights into biochar's multifaceted roles in reprogramming the rhizosphere and highlights the promise of engineering the rhizosphere through reshaping root-microbe interactions using designed biochar or root exudate cocktails. Further, given the fact that fire-derived black carbon shares similar chemistry with biochar and that increased frequency of wildfire could cause more black carbon deposition, this research spotlights the overlooked impact of fire-derived black carbon on belowground carbon and nitrogen dynamics through intricate rhizosphere interactions, which itself

requires in-depth investigation.

SUPPORTING INFORMATION

Detailed material and methods, additional results and discussion, figures (S1-S19), and tables (S1-S13) are shown in SUPPORTING INFORMATION (PDF; XLSX).

ACKNOWLEDGEMENT

This work was supported by the State University of New York College of Environmental Science and Forestry (SUNY ESF) through startup funds to Y. You. It was partially supported by the US Department of Agriculture through a McIntireStennis Capacity Grant (NI23MSCFRXXXG070). H. Yang is grateful to the ESF Alumni Association. We would like to posthumously acknowledge Kevin Guerin (ESF Analytical and Technical Services) for great assistance with fabricating acrylic mold parts on a lathe machine. We thank Dr. Alex Artyukhin for training H. Yang on the Q Exactive HF Orbitrap mass spectrometer. We thank Olivia Abry and Hayden Bregg (Department of Biology, ESF) for assistance with the EcoFAB experiment, and Dr. Leanne Powers (Department of Chemistry, ESF) for assistance with DOC measurement. We are grateful to Syracuse University Research Computing for providing high-performance computing resources.

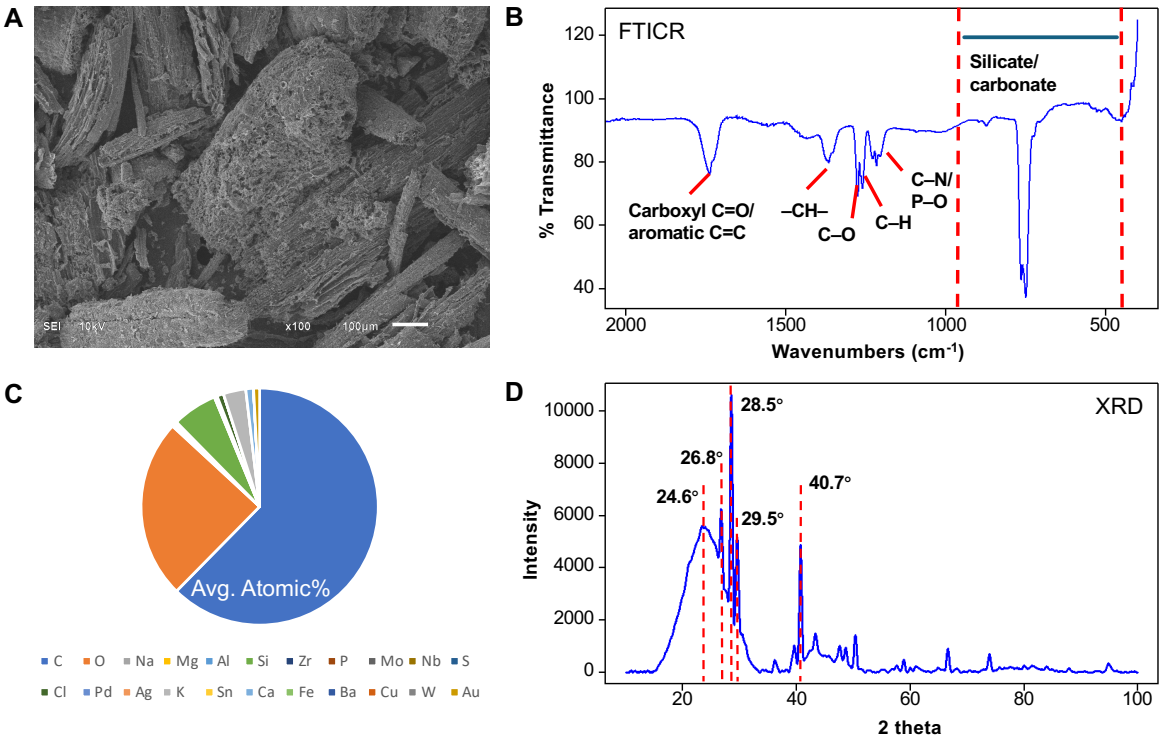

Fig 1. Physicochemical properties of the wheat biochar used in this study. (A) An representative SEM image at 100´ magnification. White scale bar indicates 100 mm. (B) FTIR spectrum in the range 400-2000 cm^{-1} with annotations of characteristic absorbance peaks. Full spectrum (400-4000 cm^{-1}) is in **Fig S3**. (C) EDS-derived elemental distribution on biochar surface. Pie chart indicates atomic percentages averaged from 29 subsamples. (D) XRD spectrum with characteristics diffraction angles highlighted.

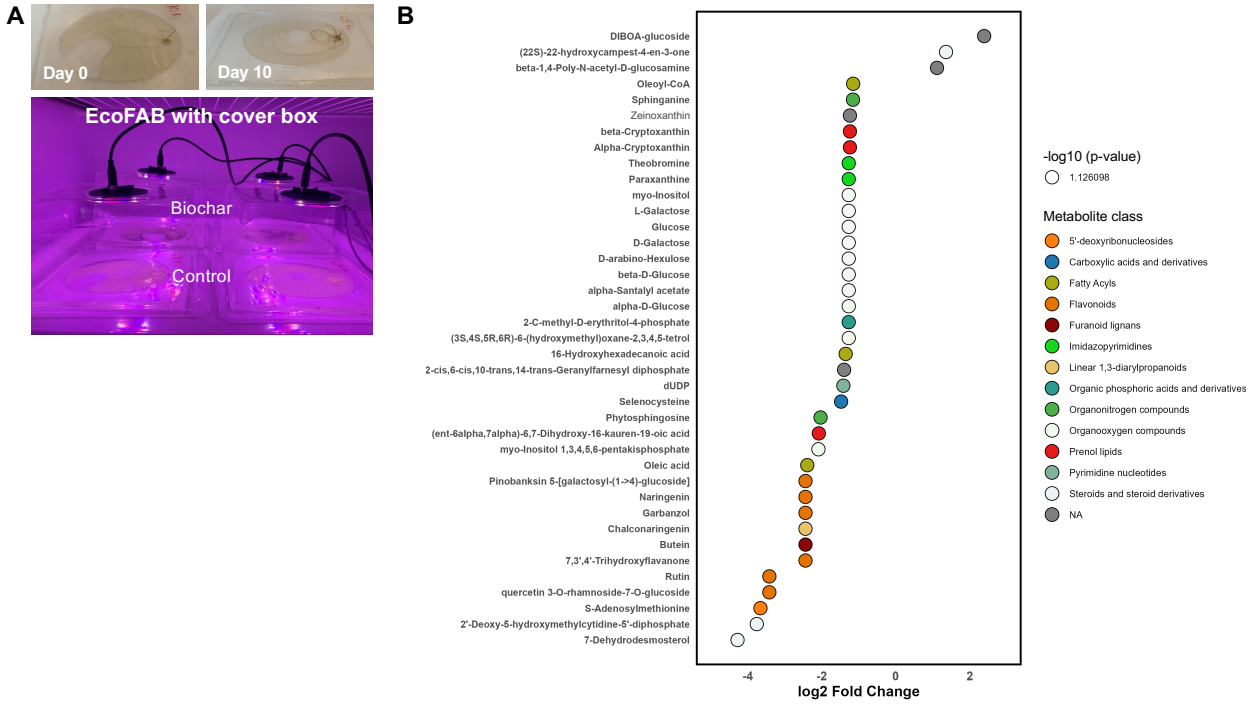

Fig 2. (A) Seedlings grown in EcoFAB devices. (B) Thirty-nine most discriminative root exudates in biochar-treated wheat roots ($|Log_2FC| > 1$, *p-adjusted* < 0.05). Individual compounds are grouped into ChemOnt classes.

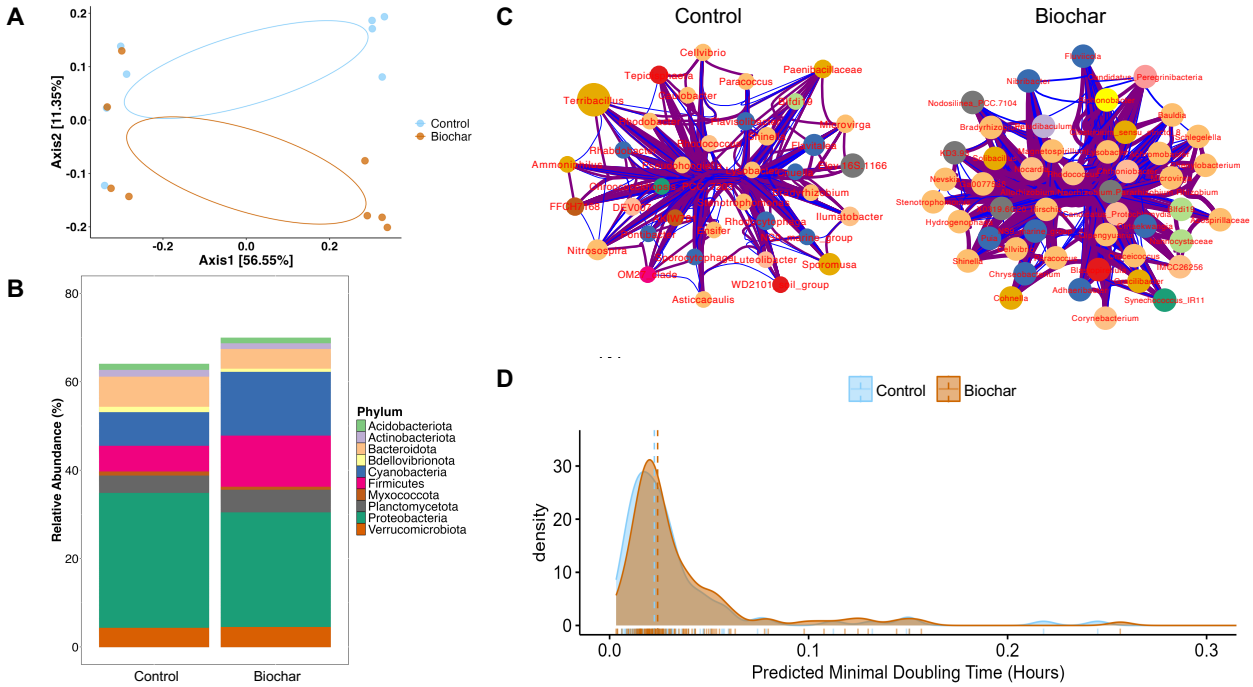

Fig 3. (A) PCoA plot of the native and biochar-treated rhizosphere microbiomes (experiment round and treatment along the first and second coordinate, respectively) (PERMANOVA test: $p < 0.05$ for round x treatment). (B) Relative abundance of the top 10 microbial phyla. (C) Hub networks of keystone genera in the native and biochar-treated rhizosphere ($p < 0.05$, 1000 bootstrapping). Node colors and sizes indicate phyla and betweenness values, respectively. Purple and blue edges indicate positive and negative correlations. (D) Biochar-rewired rhizosphere microbiome had slightly slower growth rate (i.e., larger median predicted minimum doubling time (mPMDT)) than the native rhizosphere microbiome. Prediction was made using gRodon based on enriched taxa identified using DESeq2 ($|Log_2FC| > 1$, *p-adjusted* < 0.05).

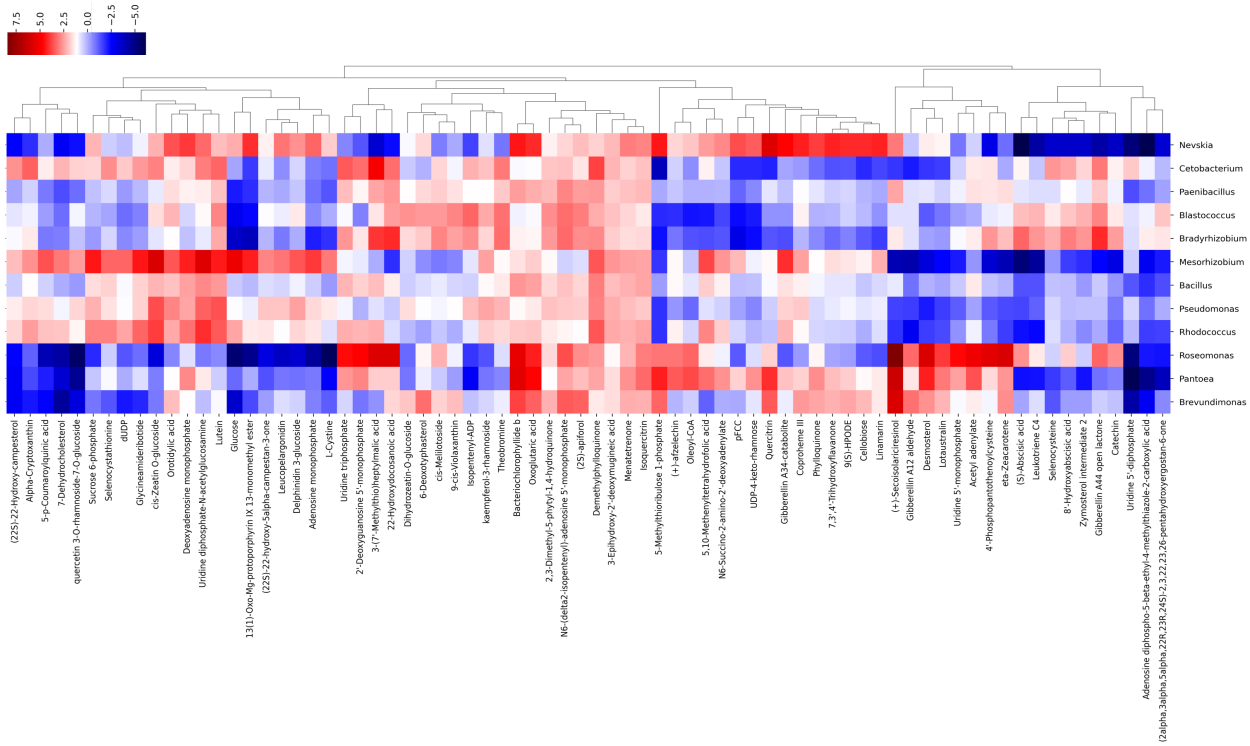

Fig 4. Associations between exudate compounds (column) and bacterial genera (row) inferred by the mmvec neural network. Colors indicate the estimated log conditional probability (i.e., association strength) of observing a root exudate compound given the presence of a microbial genus. Only those genera identified by both the OmicsNet 2.0 and mmvec approaches are shown here to ensure true positivity. Root exudates are clustered based on their associations on microbial genera.

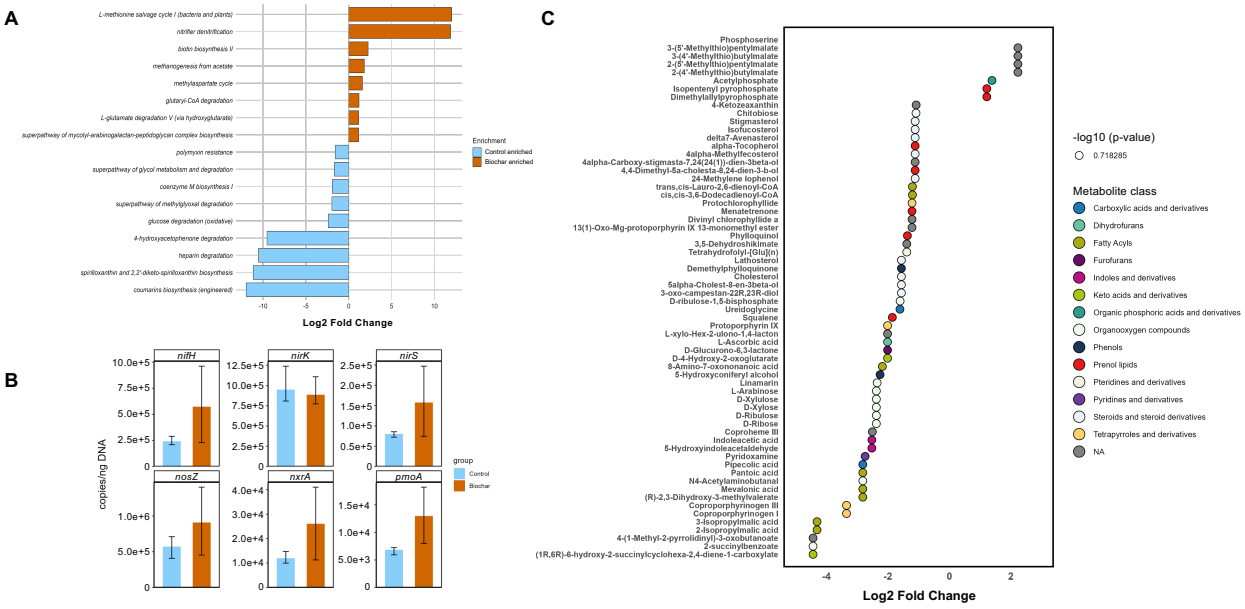

Fig 5. (A) Microbial pathways significantly regulated by biochar ($|Log_2FC| > 1$, *p-adjusted* < 0.05). Pathways were inferred using PICRUSt2. (B) qPCR-measured abundance of key nitrogen- and methane-cycling genes. Boxplots represent the median and interquartile range (IQR) of gene abundance between groups. (C) Rhizosphere soil exometabolites were significantly influenced by biochar ($|Log_2FC| > 1$, *p-adjusted* < 0.05). Individual compounds are grouped into ChemOnt classes.

REFERENCES

(1) Matson, P. A.; Parton, W. J.; Power, A. G.; Swift, M. J. Agricultural intensification and ecosystem properties. *Science* **1997**, *277* (5325), 504-509.

(2) Kerner, P.; Struhs, E.; Mirkouei, A.; Aho, K.; Lohse, K. A.; Dungan, R. S.; You, Y. Q. Microbial responses to biochar soil amendment and influential factors: a three-Level meta-analysis. *Environ. Sci. Technol.* **2023**, *57* (48), 19838-19848.

(3) Das, S. K.; Ghosh, G. K.; Avasthe, R. Biochar application for environmental management and toxic pollutant remediation. *Biomass Convers. Biorefin.* **2020**, 555-566.

(4) Hersh, B.; Mirkouei, A.; Sessions, J.; Rezaie, B.; You, Y. A review and future directions on enhancing sustainability benefits across food-energy-water systems: the potential role of biochar-derived products. *AIMS Environ. Sci.* **2019**, *6* (5), 379-416.

(5) Chen, L. J.; Jiang, Y. J.; Liang, C.; Luo, Y.; Xu, Q. S.; Han, C.; Zhao, Q. G.; Sun, B. Competitive interaction with keystone taxa induced negative priming under biochar amendments. *Microbiome* **2019**, *7*, 77.

(6) Vandenkoornhuyse, P.; Quaiser, A.; Duhamel, M.; Le Van, A.; Dufresne, A. The importance of the microbiome of the plant holobiont. *New Phytol.* **2015**, *206* (4), 1196-1120.

(7) Brtnicky, M.; Datta, R.; Holatko, J.; Bielska, L.; Gusiatin, Z. M.; Kucerik, J.; Hammerschmiedt, T.; Danish, S.; Radziemska, M.; Mravcova, L.; et al. A critical review of the possible adverse effects of biochar in the soil environment. *Sci. Total Environ.* **2021**, *796* (18), 148756.

(8) Mahmud, K.; Missaoui, A.; Lee, K. D.; Ghimire, B.; Presley, H. W.; Makaju, S. Rhizosphere microbiome manipulation for sustainable crop production. *Curr. Plant Biol.* **2021**, *27* (17), 100210.

(9) Trivedi, P.; Leach, J. E.; Tringe, S. G.; Sa, T.; Singh, B. K. Plant–microbiome interactions: from community assembly to plant health. *Nat. Rev. Microbiol.* **2020**, *18* (11), 607-621.

(10) Yang, H.; Kerner, P.; Liang, X.; Struhs, E.; Mirkouei, A.; You, Y. Biochar amendment modulates root metabolome and rhizosphere microbiome of wheat. *Biochar* **2025**, *7* (1), 46.

(11) Liu, Y.; Zhang, H.; Wang, J.; Gao, W.; Sun, X.; Xiong, Q.; Shu, X.; Miao, Y.; Shen, Q.; Xun, W. Nonpathogenic Pseudomonas syringae derivatives and its metabolites trigger the plant “cry for help” response to assemble disease suppressing and growth promoting rhizomicrobiome. *Nat. Commun.* **2024**, *15* (1), 1907.

(12) Luo, J.; Gu, S.; Guo, X.; Liu, Y.; Tao, Q.; Zhao, H.-P.; Liang, Y.; Banerjee, S.; Li, T. Core microbiota in the rhizosphere of heavy metal accumulators and its contribution to plant performance. *Environ. Sci. Technol.* **2022**, *56* (18), 12975-12987.

(13) Klimasmith, I. M.; Kent, A. D. Micromanaging the nitrogen cycle in agroecosystems. *Trends Microbiol.* **2022**, *30* (11), 1045-1055.

(14) Xiao, Z.; Rasmann, S.; Yue, L.; Lian, F.; Zou, H.; Wang, Z. The effect of biochar amendment on N-cycling genes in soils: A meta-analysis. *Sci. Total Environ.* **2019**, *696*, 133984.

(15) Liu, X.; Shi, Y.; Zhang, Q.; Li, G. Effects of biochar on nitrification and denitrification-mediated N 2 O emissions and the associated microbial community in an agricultural soil. *Environ. Sci. Pollut. Res.* **2021**, *28*, 6649-6663.

(16) Lyu, H.; Zhang, H.; Chu, M. W.; Zhang, C. F.; Tang, J. C.; Chang, S. X.; Masek, O.; Ok, Y. S. Biochar affects greenhouse gas emissions in various environments: A critical review. *Land*

Degradation & Development **2022**, *33* (17), 3327-3342.
(17) Coskun, D.; Britto, D. T.; Shi, W. M.; Kronzucker, H. J. How plant root exudates shape the nitrogen cycle. *Trends Plant Sci.* **2017**, *22* (8), 661-673.
(18) Lei, X.; Shen, Y. T.; Zhao, J. N.; Huang, J. J.; Wang, H.; Yu, Y.; Xiao, C. W. Root exudates mediate the processes of soil organic carbon input and efflux. *Plants-Basel* **2023**, *12* (3), 630.
(19) Sasse, J.; Kant, J.; Cole, B. J.; Klein, A. P.; Arsova, B.; Schlaepfer, P.; Gao, J.; Lewald, K.; Zhalnina, K.; Kosina, S. Multilab EcoFAB study shows highly reproducible physiology and depletion of soil metabolites by a model grass. *New Phytol.* **2019**, *222* (2), 1149-1160.
(20) Zengler, K.; Hofmockel, K.; Baliga, N. S.; Behie, S. W.; Bernstein, H. C.; Brown, J. B.; Dinneny, J. R.; Floge, S. A.; Forry, S. P.; Hess, M.; et al. EcoFABs: advancing microbiome science through standardized fabricated ecosystems. *Nat. Methods* **2019**, *16* (7), 567-571.
(21) Gao, J.; Sasse, J.; Lewald, K. M.; Zhalnina, K.; Cornmesser, L. T.; Duncombe, T. A.; Yoshikuni, Y.; Vogel, J. P.; Firestone, M. K.; Northen, T. R. Ecosystem fabrication (EcoFAB) protocols for the construction of laboratory ecosystems designed to study plant-microbe interactions. *JoVE (Journal of Visualized Experiments)* **2018**, (134), e57170.
(22) You, Y.; Kerner, P.; Shanmugam, S.; Khodakovskaya, M. V. Emerging investigator series: differential effects of carbon nanotubes and graphene on the tomato rhizosphere microbiome. *Environ. Sci.: Nano* **2023**, *10* (6), 1570-1584.
(23) Yang, H.; Wang, C.; Chen, F.; Yue, L.; Cao, X.; Li, J.; Zhao, X.; Wu, F.; Wang, Z.; Xing, B. Foliar carbon dot amendment modulates carbohydrate metabolism, rhizospheric properties and drought tolerance in maize seedling. *Sci. Total Environ.* **2022**, *809*, 151105.
(24) Scheltema, R. A.; Hauschild, J.-P.; Lange, O.; Hornburg, D.; Denisov, E.; Damoc, E.; Kuehn, A.; Makarov, A.; Mann, M. The Q Exactive HF, a Benchtop mass spectrometer with a pre-filter, high-performance quadrupole and an ultra-high-field Orbitrap analyzer. *Mol. Cell. Proteomics* **2014**, *13* (12), 3698-3708.
(25) Pang, Z.; Zhou, G.; Ewald, J.; Chang, L.; Hacariz, O.; Basu, N.; Xia, J. Using MetaboAnalyst 5.0 for LC–HRMS spectra processing, multi-omics integration and covariate adjustment of global metabolomics data. *Nat. Protoc.* **2022**, *17* (8), 1735-1761.
(26) Schmid, R.; Heuckeroth, S.; Korf, A.; Smirnov, A.; Myers, O.; Dyrlund, T. S.; Bushuiev, R.; Murray, K. J.; Hoffmann, N.; Lu, M.; et al. Integrative analysis of multimodal mass spectrometry data in MZmine 3. *Nat. Biotechnol.* **2023**, *41* (4), 447-449.
(27) Tautenhahn, R.; Patti, G. J.; Rinehart, D.; Siuzdak, G. XCMS online: a web-based platform to process untargeted metabolomic data. *Anal. Chem.* **2012**, *84* (11), 5035-5039.
(28) Djoumbou Feunang, Y.; Eisner, R.; Knox, C.; Chepelev, L.; Hastings, J.; Owen, G.; Fahy, E.; Steinbeck, C.; Subramanian, S.; Bolton, E. ClassyFire: automated chemical classification with a comprehensive, computable taxonomy. *J. Cheminf.* **2016**, *8* (1), 61.
(29) Oksanen, J.; Blanchet, F.; Kindt, R.; Legendre, P.; Minchin, P.; O'hara, R.; Simpson, G.; Solymos, P.; Stevens, M.; Wagner, H. Package 'vegan'. Community ecology package, version 2. *The comprehensive R network (CRAN).* **2013**.
(30) Langfelder, P.; Horvath, S. WGCNA: an R package for weighted correlation network analysis. *BMC Bioinformatics* **2008**, *9*, 559.

(31) Csardi, G.; Nepusz, T. The igraph software package for complex network research. *InterJournal, complex systems* **2006**, *1695* (5), 1-9.
(32) Douglas, G. M.; Maffei, V. J.; Zaneveld, J. R.; Yurgel, S. N.; Brown, J. R.; Taylor, C. M.; Huttenhower, C.; Langille, M. G. PICRUSt2 for prediction of metagenome functions. *Nat. Biotechnol.* **2020**, *38* (6), 685-688.
(33) Yang, C.; Mai, J.; Cao, X.; Burberry, A.; Cominelli, F.; Zhang, L. ggpicrust2: an R package for PICRUSt2 predicted functional profile analysis and visualization. *Bioinformatics* **2023**, *39* (8), btad470.
(34) López, J. L.; Fourie, A.; Poppeliers, S. W. M.; Pappas, N.; Sánchez-Gil, J. J.; de Jonge, R.; Dutilh, B. E. Growth rate is a dominant factor predicting the rhizosphere effect. *Isme J.* **2023**, *17* (9), 1396-1405.
(35) Weissman, J. L.; Hou, S.; Fuhrman, J. A. Estimating maximal microbial growth rates from cultures, metagenomes, and single cells via codon usage patterns. *Proc. Natl. Acad. Sci. U.S.A.* **2021**, *118* (12), e2016810118.
(36) Friedman, J.; Alm, E. J. Inferring correlation networks from genomic survey data. **2012,** *PLoS Comput Biol* 8(9): e1002687.
(37) Ning, D.; Wang, Y.; Fan, Y.; Wang, J.; Van Nostrand, J. D.; Wu, L.; Zhang, P.; Curtis, D. J.; Tian, R.; Lui, L.; et al. Environmental stress mediates groundwater microbial community assembly. *Nat. Microbiol.* **2024**, *9* (2), 490-501.
(38) Stegen, J. C.; Lin, X. J.; Fredrickson, J. K.; Chen, X. Y.; Kennedy, D. W.; Murray, C. J.; Rockhold, M. L.; Konopka, A. Quantifying community assembly processes and identifying features that impose them. *Isme J.* **2013**, *7* (11), 2069-2079.
(39) Taylor, S. C.; Mrkusich, E. M. The state of RT-quantitative PCR: firsthand observations of implementation of minimum information for the publication of quantitative real-time PCR experiments (MIQE). *J. Mol. Microbiol. Biotechnol.* **2014**, *24* (1), 46-52.
(40) Burmølle, M.; Hansen, L. H.; Sørensen, S. J. Establishment and early succession of a multispecies biofilm composed of soil bacteria. *Microb. Ecol.* **2007**, *54*, 352-362.
(41) Morton, J. T.; Aksenov, A. A.; Nothias, L. F.; Foulds, J. R.; Quinn, R. A.; Badri, M. H.; Swenson, T. L.; Van Goethem, M. W.; Northen, T. R.; Vazquez-Baeza, Y.; et al. Learning representations of microbe–metabolite interactions. *Nat. Methods* **2019**, *16* (12), 1306-1314.
(42) Zhou, G.; Pang, Z.; Lu, Y.; Ewald, J.; Xia, J. OmicsNet 2.0: a web-based platform for multi-omics integration and network visual analytics. *Nucleic Acids Res.* **2022**, *50* (W1), W527-W533.
(43) Liu, L.; Liu, G.; Zhou, J.; Wang, J.; Jin, R.; Wang, A. Improved bioreduction of nitrobenzene by black carbon/biochar derived from crop residues. *RSC advances* **2016**, *6* (87), 84388-84396.
(44) Yao, S.; Li, X.; Cheng, H.; Zhang, C.; Bian, Y.; Jiang, X.; Song, Y. Resource utilization of a typical vegetable waste as biochars in removing phthalate acid esters from water: a sorption case study. *Bioresour. Technol.* **2019**, *293*, 122081.
(45) Zhou, Q.; Jiang, X.; Li, X.; Jia, C. Q.; Jiang, W. Preparation of high-yield N-doped biochar from nitrogen-containing phosphate and its effective adsorption for toluene. *RSC Advances* **2018**, *8* (53), 30171-30179.
(46) Waqas, M.; Aburiazaiza, A. S.; Miandad, R.; Rehan, M.; Barakat, M. A.; Nizami, A. S.

739 Development of biochar as fuel and catalyst in energy recovery technologies. *J. Clean. Prod.*
740 **2018**, *188*, 477-488..
741 (47) Joseph, S.; Cowie, A. L.; Van Zwieten, L.; Bolan, N.; Budai, A.; Buss, W.; Cayuela, M. L.;
742 Graber, E. R.; Ippolito, J. A.; Kuzyakov, Y. How biochar works, and when it doesn't: A review of
743 mechanisms controlling soil and plant responses to biochar. *Gcb Bioenergy* **2021**, *13* (11), 1731-
744 1764.
745 (48) Ali, I.; Ullah, S.; Iqbal, A.; Quan, Z.; Liang, H.; Ahmad, S.; Muhammad, I.; Amanullah; Imran;
746 Guo, Z.; et al. Combined application of biochar and nitrogen fertilizer promotes the activity of
747 starch metabolism enzymes and the expression of related genes in rice in a dual cropping system.
748 *BMC Plant Biol.* **2021**, *21* (1), 600.
749 (49) Kolton, M.; Graber, E. R.; Tsehansky, L.; Elad, Y.; Cytryn, E. Biochar-stimulated plant
750 performance is strongly linked to microbial diversity and metabolic potential in the rhizosphere.
751 *New Phytol.* **2017**, *213* (3), 1393-1404.
752 (50) Shamshina, J. L.; Kelly, A.; Oldham, T.; Rogers, R. D. Agricultural uses of chitin polymers.
753 *Environ. Chem. Lett.* **2020**, *18* (1), 53-60.
754 (51) Vukašinović, N.; Wang, Y.; Vanhoutte, I.; Fendrych, M.; Guo, B.; Kvasnica, M.; Jiroutová, P.;
755 Oklestkova, J.; Strnad, M.; Russinova, E. Local brassinosteroid biosynthesis enables optimal root
756 growth. *Nat. Plants* **2021**, *7* (5), 619-632.
757 (52) Yu, J.; Tu, X.; Huang, A. C. Functions and biosynthesis of plant signaling metabolites
758 mediating plant–microbe interactions. *Nat. Prod. Rep.* **2022**, *39* (7), 1393-1422.
759 (53) Cotton, T. A.; Pétriacq, P.; Cameron, D. D.; Meselmani, M. A.; Schwarzenbacher, R.; Rolfe,
760 S. A.; Ton, J. Metabolic regulation of the maize rhizobiome by benzoxazinoids. *ISME J.* **2019**, *13*
761 (7), 1647-1658.
762 (54) Hu, L.; Robert, C. A.; Cadot, S.; Zhang, X.; Ye, M.; Li, B.; Manzo, D.; Chervet, N.; Steinger,
763 T.; Van Der Heijden, M. G. Root exudate metabolites drive plant-soil feedbacks on growth and
764 defense by shaping the rhizosphere microbiota. *Nat. Commun.* **2018**, *9* (1), 2738.
765 (55) Kudjordjie, E. N.; Sapkota, R.; Steffensen, S. K.; Fomsgaard, I. S.; Nicolaisen, M. Maize
766 synthesized benzoxazinoids affect the host associated microbiome. *Microbiome* **2019**, *7* (1), 59.
767 (56) Wang, L.; Chen, M.; Lam, P.-Y.; Dini-Andreote, F.; Dai, L.; Wei, Z. Multifaceted roles of
768 flavonoids mediating plant-microbe interactions. *Microbiome* **2022**, *10* (1), 233.
769 (57) Liang, T.; Shi, C.; Peng, Y.; Tan, H.; Xin, P.; Yang, Y.; Wang, F.; Li, X.; Chu, J.; Huang, J.
770 Brassinosteroid-activated BRI1-EMS-SUPPRESSOR 1 inhibits flavonoid biosynthesis and
771 coordinates growth and UV-B stress responses in plants. *Plant cell* **2020**, *32* (10), 3224-3239.
772 (58) Biederman, L. A.; Harpole, W. S. Biochar and its effects on plant productivity and nutrient
773 cycling: a meta-analysis. *GCB bioenergy* **2013**, *5* (2), 202-214.
774 (59) Li, M.; Song, Z.; Li, Z.; Qiao, R.; Zhang, P.; Ding, C.; Xie, J.; Chen, Y.; Guo, H. Populus root
775 exudates are associated with rhizosphere microbial communities and symbiotic patterns. *Front.*
776 *Microbiol.* **2022**, *13*, 1042944.
777 (60) Macabuhay, A.; Arsova, B.; Walker, R.; Johnson, A.; Watt, M.; Roessner, U. Modulators or
778 facilitators? Roles of lipids in plant root–microbe interactions. *Trends Plant Sci.* **2022**, *27* (2), 180-
779 190.

780 (61) He, M.; Ding, N. Z. Plant unsaturated fatty acids: multiple roles in stress response. *Front.*
781 *Plant Sci.* **2020**, *11*. 562785.
782 (62) Gu, S.; Wei, Z.; Shao, Z.; Friman, V.-P.; Cao, K.; Yang, T.; Kramer, J.; Wang, X.; Li, M.; Mei,
783 X. Competition for iron drives phytopathogen control by natural rhizosphere microbiomes. *Nature*
784 *Microbiology* **2020**, *5* (8), 1002-1010.
785 (63) O'Banion, B. S.; Jones, P.; Demetros, A. A.; Kelley, B. R.; Knoor, L. H.; Wagner, A. S.; Chen,
786 J.-G.; Muchero, W.; Reynolds, T. B.; Jacobson, D. Plant myo-inositol transport influences bacterial
787 colonization phenotypes. *Curr. Biol.* **2023**, *33* (15), 3111-3124.
788 (64) Missbah El Idrissi, M.; Bouhnik, O.; ElFaik, S.; Alami, S.; Lamin, H.; Bedmar, E. J.;
789 Abdelmoumen, H. Characterization of bradyrhizobium spp. nodulating lupinus cosentinii and L.
790 luteus microsymbionts in Morocco. *Front. Agron.* **2021**, *3*, 661295.
791 (65) Hollensteiner, J.; Schneider, D.; Poehlein, A.; Brinkhoff, T.; Daniel, R. Pan-genome analysis
792 of six Paracoccus type strain genomes reveal lifestyle traits. *Plos one* **2023**, *18* (12), e0287947.
793 (66) de Bruijn, I.; Cheng, X.; de Jager, V.; Expósito, R. G.; Watrous, J.; Patel, N.; Postma, J.;
794 Dorrestein, P. C.; Kobayashi, D.; Raaijmakers, J. M. Comparative genomics and metabolic
795 profiling of the genus Lysobacter. *BMC Genomics* **2015**, *16* (1), 991.
796 (67) Kumar, A.; Rithesh, L.; Kumar, V.; Raghuvanshi, N.; Chaudhary, K.; Abhineet; Pandey, A. K.
797 Stenotrophomonas in diversified cropping systems: friend or foe? *Front. Microbiol.* **2023**, *14*,
798 1214680.
799 (68) Wang, Z.; Hu, H.; Zhang, Z.; Xu, Y.; Xu, P.; Tang, H. IA multiple PAHs-degrading Shinella sp.
800 strain and its potential bioremediation in wastewater. *Sci Total Environ* **2023**, *879*, 162974.
801 (69) Wu, Y.-R.; He, J. Characterization of a xylanase-producing Cellvibrio mixtus strain J3-8 and
802 its genome analysis. *Sci. Rep.* **2015**, *5* (1), 10521.
803 (70) Forsberg, Z.; Nelson, C. E.; Dalhus, B.; Mekasha, S.; Loose, J. S.; Crouch, L. I.; Røhr Å, K.;
804 Gardner, J. G.; Eijsink, V. G.; Vaaje-Kolstad, G. Structural and functional analysis of a lytic
805 polysaccharide monooxygenase important for efficient utilization of chitin in cellvibrio japonicus.
806 *J Biol Chem* **2016**, *291* (14), 7300-7312.
807 (71) Ma, S.; Huang, S. W.; Tian, Y.; Lu, X. Y. Heterotrophic ammonium assimilation: An important
808 driving force for aerobic denitrification of Rhodococcus erythropolis strain Y10. *Chemosphere*
809 **2022**, *291*..
810 (72) Yuzikhin, O. S.; Gogoleva, N. E.; Shaposhnikov, A. I.; Konnova, T. A.; Osipova, E. V.; Syrova,
811 D. S.; Ermakova, E. A.; Shevchenko, V. P.; Nagaev, I. Y.; Shevchenko, K. V.; et al. Rhizosphere
812 bacterium Rhodococcus sp. P1Y metabolizes abscisic acid to form dehydrovomifoliol.
813 *Biomolecules* **2021**, *11* (3), 345.
814 (73) Jara-Servin, A.; Mejia, G.; Romero, M. F.; Peimbert, M.; Alcaraz, L. D. Unravelling the
815 genomic and environmental diversity of the ubiquitous Solirubrobacter. *Environ. Microbiol.* **2024**,
816 *26* (8), e16685.
817 (74) Jung, H.; Lee, D.; Lee, S.; Kong, H. J.; Park, J.; Seo, Y.-S. Comparative genomic analysis of
818 Chryseobacterium species: deep insights into plant-growth-promoting and halotolerant capacities.
819 *Microb. Genom.* **2023**, *9* (10), 001108.
820 (75) Zhang, C.; Zhou, D.-F.; Wang, M.-Y.; Song, Y.-Z.; Zhang, C.; Zhang, M.-M.; Sun, J.; Yao, L.;

Mo, X.-H.; Ma, Z.-X. Phosphoribosylpyrophosphate synthetase as a metabolic valve advances Methylobacterium/Methylorubrum phyllosphere colonization and plant growth. *Nat. Commun.* **2024**, *15* (1), 5969.
(76) You, Y.; Aho, K.; Lohse, K. A.; Schwabedissen, S. G.; Ledbetter, R. N.; Magnuson, T. S. Biological soil crust bacterial communities vary along climatic and shrub cover gradients within a sagebrush steppe ecosystem. *Front. Microbiol.* **2021**, *12*, 569791.
(77) Lu, Y.; Rosencrantz, D.; Liesack, W.; Conrad, R. Structure and activity of bacterial community inhabiting rice roots and the rhizosphere. *Environ. Microbiol.* **2006**, *8* (8), 1351-1360.
(78) Shutsrirung, A.; Chromkaew, Y.; Pathom-Aree, W.; Choonluchanon, S.; Boonkerd, N. Diversity of endophytic actinomycetes in mandarin grown in northern Thailand, their phytohormone production potential and plant growth promoting activity. *Soil Sci. Plant Nutr.* **2013**, *59* (3), 322-330.
(79) Alotaibi, F.; St-Arnaud, M.; Hijri, M. In-depth characterization of plant growth promotion potentials of selected alkanes-degrading plant growth-promoting bacterial isolates. *Front. Microbiol.* **2022**, *13*, 863702.
(80) Ludington, W. B.; Seher, T. D.; Applegate, O.; Li, X.; Kliegman, J. I.; Langelier, C.; Atwill, E. R.; Harter, T.; DeRisi, J. L. Assessing biosynthetic potential of agricultural groundwater through metagenomic sequencing: A diverse anammox community dominates nitrate-rich groundwater. *PLoS One* **2017**, *12* (4), e0174930.
(81) Radhakrishnan, N.; Krishnasamy, C. Isolation and characterization of salt-stress-tolerant rhizosphere soil bacteria and their effects on plant growth-promoting properties. *Sci. Rep.* **2024**, *14* (1), 24909.
(82) Kaur, M.; Karnwal, A. Screening of plant growth-promoting attributes bearing endogenous bacteria from abiotic stress resisting high altitude plants. *J. Agric. Food Res.* **2023**, *11*, 100489.
(83) Venturi, V.; Keel, C. Signaling in the rhizosphere. *Trends Plant Sci.* **2016**, *21* (3), 187-198.
(84) Tzipilevich, E.; Russ, D.; Dangl, J. L.; Benfey, P. N. Plant immune system activation is necessary for efficient root colonization by auxin-secreting beneficial bacteria. *Cell host & microbe* **2021**, *29* (10), 1507-1520. e1504.
(85) Banerjee, S.; Schlaeppi, K.; van der Heijden, M. G. A. Keystone taxa as drivers of microbiome structure and functioning. *Nat. Rev. Microbiol.* **2018**, *16* (9), 567-576.
(86) Marschmann, G. L.; Tang, J.; Zhalnina, K.; Karaoz, U.; Cho, H.; Le, B.; Pett-Ridge, J.; Brodie, E. L. Predictions of rhizosphere microbiome dynamics with a genome-informed and trait-based energy budget model. *Nat. Microbiol.* **2024**, *9* (2), 421-433.
(87) Zhalnina, K.; Louie, K. B.; Hao, Z.; Mansoori, N.; Da Rocha, U. N.; Shi, S.; Cho, H.; Karaoz, U.; Loqué, D.; Bowen, B. P. Dynamic root exudate chemistry and microbial substrate preferences drive patterns in rhizosphere microbial community assembly. *Nat. Microbiol.* **2018**, *3* (4), 470-480.
(88) Thoenen, L.; Giroud, C.; Kreuzer, M.; Waelchli, J.; Gfeller, V.; Deslandes-Hérold, G.; Mateo, P.; Robert, C. A. M.; Ahrens, C. H.; Rubio-Somoza, I.; et al. Bacterial tolerance to host-exuded specialized metabolites structures the maize root microbiome. *Proc. Natl. Acad. Sci. U.S.A.* **2023**, *120* (44), e2310134120.
(89) Freire-Zapata, V.; Holland-Moritz, H.; Cronin, D. R.; Aroney, S.; Smith, D. A.; Wilson, R. M.;

Ernakovich, J. G.; Woodcroft, B. J.; Bagby, S. C.; 13, E. F. T. H. S. B. M. R. Microbiome–metabolite linkages drive greenhouse gas dynamics over a permafrost thaw gradient. *Nat. Microbiol.* **2024**, *9* (11), 2892-2908.

(90) Orozco-Mosqueda, M. D.; Santoyo, G.; Glick, B. R. Recent advances in the bacterial phytohormone modulation of plant growth. *Plants-Basel* **2023**, *12* (3). 606.

(91) Lin, H.; Chang, J. J.; Liang, T. N.; Yang, C.; Wei, Y. Y.; Peng, W.; Xu, A. K.; Duan, C. Q.; Zhao, Y. G. Effects of norfloxacin on the interaction between duckweed and its growth-promoting bacterial assemblages. *J. Hazard. Mater.* **2025**, *492*. 138249.

(92) Nascimento, F. X.; Hernandez, A. G.; Glick, B. R.; Rossi, M. J. The extreme plant-growth-promoting properties of Pantoea phytobeneficialis MSR2 revealed by functional and genomic analysis. *Environ. Microbiol.* **2020**, *22* (4), 1341-1355.

(93) Nett, R. S.; Montanares, M.; Marcassa, A.; Lu, X.; Nagel, R.; Charles, T. C.; Hedden, P.; Rojas, M. C.; Peters, R. J. Elucidation of gibberellin biosynthesis in bacteria reveals convergent evolution. *Nat. Chem. Biol.* **2017**, *13* (1), 69-74.

(94) Hartmann, M.; Six, J. Soil structure and microbiome functions in agroecosystems. *Nat. Rev. Earth Environ.* **2023**, *4* (1), 4-18.

(95) Nett, R. S.; Contreras, T.; Peters, R. J. Characterization of CYP115 as a gibberellin 3-oxidase indicates that certain rhizobia can produce bioactive gibberellin A4. *ACS Chem. Biol.* **2017**, *12* (4), 912-917.

(96) Pang, Z.; Chen, J.; Wang, T.; Gao, C.; Li, Z.; Guo, L.; Xu, J.; Cheng, Y. Linking plant secondary metabolites and plant microbiomes: a review. *Front. Plant Sci.* **2021**, *12*, 621276.

(97) Boiero, L.; Perrig, D.; Masciarelli, O.; Penna, C.; Cassán, F.; Luna, V. Phytohormone production by three strains of Bradyrhizobium japonicum and possible physiological and technological implications. *Appl. Microbiol. Biotechnol.* **2007**, *74* (4), 874-880.

(98) Eichmann, R.; Richards, L.; Schäfer, P. Hormones as go-betweens in plant microbiome assembly. *Plant J.* **2021**, *105* (2), 518-541.

(99) Pertry, I.; Václavíková, K.; Depuydt, S.; Galuszka, P.; Spíchal, L.; Temmerman, W.; Stes, E.; Schmülling, T.; Kakimoto, T.; Van Montagu, M. C. Identification of Rhodococcus fascians cytokinins and their modus operandi to reshape the plant. *Proc. Natl. Acad. Sci. U.S.A.* **2009**, *106* (3), 929-934.

(100) Yin, L.-Z.; Li, J.-L.; Fang, B.-Z.; Liu, Z.-T.; Wang, P.; Dong, L.; Duan, L.; Luo, X.-Q.; Li, S.-H.; Li, W.-J. Roseomonas ponticola sp. nov., a novel bacterium isolated from Pearl River estuary. *Int. J. Syst. Evol. Microbiol.* **2021**, *71* (10), 004994.

(101) Kuypers, M. M.; Marchant, H. K.; Kartal, B. The microbial nitrogen-cycling network. *Nat. Rev. Microbiol.* **2018**, *16* (5), 263-276.

(102) Zhang, X.; Qiu, Y.; Gilliam, F. S.; Gillespie, C. J.; Tu, C.; Reberg-Horton, S. C.; Hu, S. Arbuscular mycorrhizae shift community composition of N-cycling microbes and suppress soil N_2O emission. *Environ. Sci. Technol.* **2022**, *56* (18), 13461-13472.

(103) Cayuela, M. L.; Sánchez-Monedero, M. A.; Roig, A.; Hanley, K.; Enders, A.; Lehmann, J. Biochar and denitrification in soils: when, how much and why does biochar reduce N_2O emissions? *Sci. Rep.* **2013**, *3* (1), 1732.

(104) Shan, J.; Sanford, R. A.; Chee-Sanford, J.; Ooi, S. K.; Löffler, F. E.; Konstantinidis, K. T.; Yang, W. H. Beyond denitrification: the role of microbial diversity in controlling nitrous oxide reduction and soil nitrous oxide emissions. *Glob. Change Biol.* **2021**, *27* (12), 2669-2683.
(105) Li, Y.; Katzmann, E.; Borg, S.; Schüler, D. The periplasmic nitrate reductase Nap is required for anaerobic growth and involved in redox control of magnetite biomineralization in Magnetospirillum gryphiswaldense. *J. Bacteriol.* **2012**, *194* (18), 4847-4856.
(106) He, G.; Wang, W.; Chen, G.; Xie, Y.; Parks, J. M.; Davin, M. E.; Hettich, R. L.; Konstantinidis, K. T.; Löffler, F. E. A novel bacterial protein family that catalyses nitrous oxide reduction. *Nature* **2025**, *646*, 152–160.
(107) Garcia, P. S.; Gribaldo, S.; Borrel, G. Diversity and evolution of methane-related pathways in archaea. *Annu. Rev. Microbiol.* **2022**, *76*, 727-755.
(108) Nazaries, L.; Murrell, J. C.; Millard, P.; Baggs, L.; Singh, B. K. Methane, microbes and models: fundamental understanding of the soil methane cycle for future predictions. *Environ. Microbiol.* **2013**, *15* (9), 2395-2417.